NASA TECHNICAL REPORT

NASA TR R-268



NASA TR R-268

# NUMERICAL RESULTS FOR THE DIFFRACTION OF A NORMAL SHOCK WAVE BY A SPHERE AND FOR THE SUBSEQUENT TRANSIENT FLOW

*by Richard W. Barnwell*

*Langley Research Center*
*Langley Station, Hampton, Va.*

NATIONAL AERONAUTICS AND SPACE ADMINISTRATION • WASHINGTON, D. C. • SEPTEMBER 1967

# NUMERICAL RESULTS FOR THE DIFFRACTION OF A NORMAL SHOCK WAVE BY A SPHERE AND FOR THE SUBSEQUENT TRANSIENT FLOW

By Richard W. Barnwell

Langley Research Center
Langley Station, Hampton, Va.

NATIONAL AERONAUTICS AND SPACE ADMINISTRATION

For sale by the Clearinghouse for Federal Scientific and Technical Information
Springfield, Virginia 22151 – CFSTI price $3.00

# NUMERICAL RESULTS FOR THE DIFFRACTION OF A NORMAL SHOCK WAVE BY A SPHERE AND FOR THE SUBSEQUENT TRANSIENT FLOW

By Richard W. Barnwell
Langley Research Center

## SUMMARY

The finite-difference method which Peter D. Lax developed for treating unsteady inviscid flow fields is used to study the transient flow in the shock layer of a sphere that has been struck by a normal shock wave. Transient flow of this sort is encountered when a shock tube is used as a supersonic wind tunnel. Time histories of the shock detachment distance and the stagnation-point pressure and tangential velocity gradient are presented for ranges of the incident-shock Mach number and the perfect-gas specific-heat ratio. These results show that the stagnation-point pressure approaches the steady value much more rapidly than the shock detachment distance. In general, the stagnation-point tangential velocity gradient approaches the steady value less rapidly than stagnation-point pressure but more rapidly than the shock detachment distance. As the specific-heat ratio is decreased and the incident-shock Mach number is increased, the variation of the velocity gradient with respect to the shock detachment distance becomes more nearly linear.

## INTRODUCTION

Supersonic flow about a model mounted in a shock tube is initiated by causing a normal shock wave to travel down the tube past the model. When the shock strikes the model it is diffracted, and a shock layer is formed ahead of the model. This shock layer adjusts with time until steady flow is established.

Several investigators have obtained approximate analytical expressions for the time history of the shock detachment distance for a blunt model which has been washed by a normal shock by assuming that the model is placed in a still gas and accelerated instantaneously to supersonic speed. Cabannes (ref. 1) has developed a second-order Taylor series expansion for smooth plane and axisymmetric blunt bodies. Bausset (ref. 2) has obtained the third- and fourth-order terms for this expansion and has included three-dimensional effects. Miles, Mirels, and Wang (ref. 3) have used a mass-balance treatment for the special case of the flat-nosed cylinder.

Experimental results have been obtained for the transient behavior in the flow fields of various blunt bodies which have been washed by normal shocks. Results have been presented by Davies (ref. 4) for flat-nosed cylinders with rounded corners. In addition, he has derived an expression for the time variation of the shock-layer thickness by assuming that the bow-shock deceleration is constant. Offenhartz and Weisblatt (ref. 5) have obtained data for circular cylinders alined with the flow with several nose bluntnesses. Some results for cylinders with axes perpendicular to the flow and for spheres have been published in references 6, 7, and 8.

Numerical results for diffraction of normal shock waves by flat-nosed cylinders coaxial with the flow have been obtained by Butler (ref. 9).

In this report numerical results are presented for the time histories of the shock detachment distance and the stagnation-point pressure and tangential velocity gradient for a sphere which has been washed by a normal shock wave. The flow field is assumed to be inviscid, and a calorically perfect gas model is employed. The cases which are treated cover a wide range of incident-shock Mach number and specific-heat ratio. A finite-difference method based on a technique of first-order accuracy which Lax (ref. 10) developed for treating one-dimensional inviscid unsteady flow fields containing shock waves is used to calculate the results. The Lax technique is used to make blunt-body flow-field calculations in references 11 and 12. Other applications of the Lax technique are given in references 13 and 14.

## SYMBOLS

$A_i, B_i, C_i, D_i, E_i$ quantities defined by equations (10)

$a$ speed of sound

$c$ speed of reflected shock wave for one-dimensional shock reflection problem

$K$ constant defined by equations (11)

$K_1$ constant defined by equations (14)

$M_s$ incident-shock-wave Mach number

$M$ Mach number

$p$ pressure

| | |
|---|---|
| r | radial distance from center of sphere |
| t | time |
| u | radial velocity component |
| V | total magnitude of velocity |
| v | tangential velocity component |
| $\alpha$ | constant defined by equation (A8) |
| $\gamma$ | perfect-gas specific-heat ratio |
| $\Delta t, \Delta r, \Delta\theta$ | mesh spacings |
| $\delta$ | shock detachment distance |
| $\theta$ | angular coordinate measured from axis of symmetry |
| $\nu$ | constant defined by equations (9) |
| $\rho$ | mass density |
| $\tau$ | nondimensional time defined by equation (17) |

Subscripts:

| | |
|---|---|
| b | at the body surface |
| $l$ | spatial position, $r = r_b + (l - 1)\Delta r$ |
| m | spatial position, $\theta = (m - 1)\Delta\theta$ |
| max | maximum |
| rs | quantity evaluated behind the reflected shock at the point where a normal shock wave is diffracted by a surface |

| | |
|---|---|
| S | steady flow |
| s | at the shock |
| stag | at the stagnation point |
| $\bar{t} = 0$ | immediately after shock impingement |
| $\infty$ | free stream |

Superscript:

| | |
|---|---|
| k | number of time steps, $t = k\,\Delta t$ |

A prime denotes differentiation with respect to $\theta$.

A bar denotes a nondimensional quantity as given by equations (A4).

## PROBLEM DESCRIPTION

The transient behavior which occurs when a normal shock wave moves into a still gas and strikes a sphere is to be investigated. The flow field is considered to be inviscid, and a calorically perfect gas model is assumed. Phenomena which are treated include the diffraction of the incident shock wave by the sphere and the unsteady flow in the shock layer ahead of the body after shock impingement and before the establishment of steady flow.

Numerical solutions are obtained to the initial-value problem for the partial differential equations which govern unsteady inviscid gas flow and the boundary conditions for flow over a sphere. The flow properties are determined at successive instants in time at points fixed in the flow field.

### Governing Equations

The natural coordinate system for treating flow about a sphere is a spherical polar system with its origin at the center of the sphere. Since the flow is symmetric about the normal to the incident shock wave which passes through the center of the sphere, the axis of the coordinate system is chosen to lie along this line. The flow properties are functions of the distance from the center of the sphere $r$, the polar angle $\theta$, and the time $t$.

The usual conservation form of the governing equations for unsteady axisymmetric flow in terms of spherical polar coordinates is given in reference 11. As is pointed out

in that reference, this form of the governing equations cannot be used to evaluate the flow properties along the axis where $\theta$ and $\sin\theta$ are equal to zero. A useful conservation form of the equations for application along the axis is obtained by dividing the equations in reference 11 by $r \sin\theta$, the perpendicular distance from the axis, and evaluating the indeterminate terms which result with the aid of l'Hospital's rule.

When the equations of reference 11 are divided by $r \sin\theta$, the following equations result:

Continuity:

$$\frac{\partial(\rho r)}{\partial t} + \frac{\partial(\rho u r)}{\partial r} + \frac{\partial(\rho v)}{\partial \theta} + \rho u + \rho v \cot\theta = 0 \tag{1}$$

Radial momentum:

$$\frac{\partial(\rho u r)}{\partial t} + \frac{\partial}{\partial r}\left[\left(p + \rho u^2\right) r\right] + \frac{\partial(\rho u v)}{\partial \theta} - \left[p - \rho\left(u^2 - v^2\right)\right] + \rho u v \cot\theta = 0 \tag{2}$$

Tangential momentum:

$$\frac{\partial(\rho v r)}{\partial t} + \frac{\partial}{\partial r}(\rho u v r) + \frac{\partial}{\partial \theta}\left(p + \rho v^2\right) + 2\rho u v + \rho v^2 \cot\theta = 0 \tag{3}$$

Energy:

$$\frac{\partial}{\partial t}\left\{\left[\frac{1}{\gamma - 1} p + \frac{1}{2}\rho\left(u^2 + v^2\right)\right] r\right\} + \frac{\partial}{\partial r}\left\{u\left[\frac{\gamma}{\gamma - 1} p + \frac{1}{2}\rho\left(u^2 + v^2\right)\right] r\right\} + \frac{\partial}{\partial \theta}\left\{v\left[\frac{\gamma}{\gamma - 1} p\right.\right.$$

$$\left.\left. + \frac{1}{2}\rho\left(u^2 + v^2\right)\right]\right\} + u\left[\frac{\gamma}{\gamma - 1} p + \frac{1}{2}\rho\left(u^2 + v^2\right)\right] + v\left[\frac{\gamma}{\gamma - 1} p + \frac{1}{2}\rho\left(u^2 + v^2\right)\right]\cot\theta = 0 \tag{4}$$

In this report these equations are used for all values of $\theta$ except $\theta = 0$, where the terms containing the product $v \cot\theta$ are indeterminate. As previously mentioned, l'Hospital's rule is used to evaluate these indeterminate forms. The governing equations for use when $\theta = 0$ are written as:

Continuity:

$$\frac{\partial(\rho r)}{\partial t} + \frac{\partial(\rho u r)}{\partial r} + 2\frac{\partial(\rho v)}{\partial \theta} + \rho u = 0 \tag{5}$$

Radial momentum:

$$\frac{\partial}{\partial t}(\rho u r) + \frac{\partial}{\partial r}\left[(p + \rho u^2)r\right] + 2\frac{\partial}{\partial \theta}(\rho uv) - \left[p - \rho(u^2 - v^2)\right] = 0 \tag{6}$$

Energy:

$$\frac{\partial}{\partial t}\left\{\left[\frac{1}{\gamma - 1}p + \frac{1}{2}\rho(u^2 + v^2)\right]r\right\} + \frac{\partial}{\partial r}\left\{u\left[\frac{\gamma}{\gamma - 1}p + \frac{1}{2}\rho(u^2 + v^2)\right]r\right\}$$

$$+ 2\frac{\partial}{\partial \theta}\left\{v\left[\frac{\gamma}{\gamma - 1}p + \frac{1}{2}\rho(u^2 + v^2)\right]\right\} + u\left[\frac{\gamma}{\gamma - 1}p + \frac{1}{2}\rho(u^2 + v^2)\right] = 0 \tag{7}$$

The tangential momentum equation is not needed when $\theta = 0$ because the tangential velocity component is known to have a value of zero on the axis.

## Boundary Conditions

The computational region which is used in this report is shown in figure 1. It is bounded by two circular arcs and two radial lines. Along the arc $r = r_b$, which

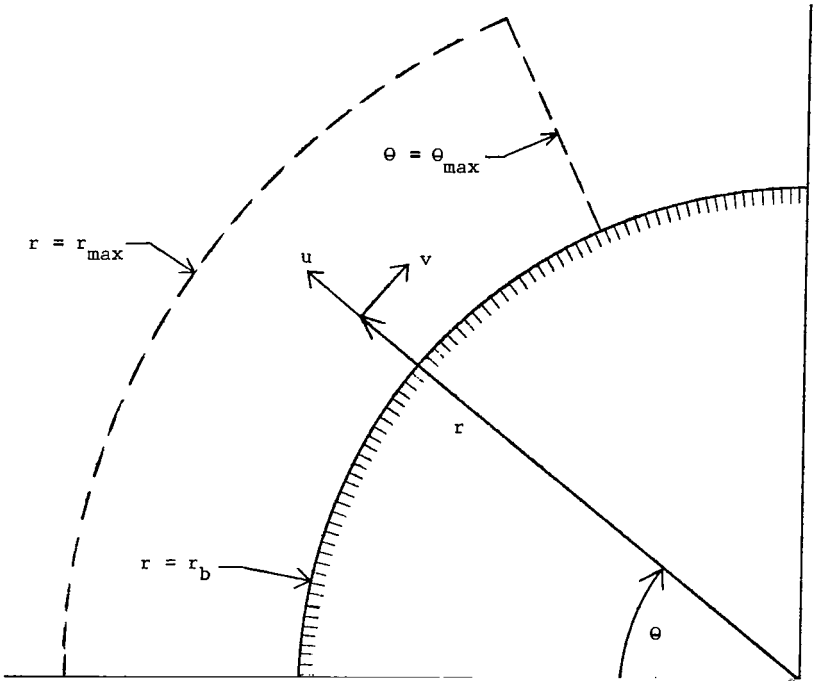


Figure 1.- Computational region.

represents the surface of the sphere, the condition $u = 0$ is applied since the flow direction must be tangent to the surface at the body. Along the axis, where $\theta = 0$, the symmetry condition $v = 0$ is applied. The arc $r = r_{max}$ is positioned so that it lies outside the steady-shock layer. The line $\theta = \theta_{max}$ is positioned so that the flow at points in its vicinity is supersonic at all times after the incident shock wave has passed out of the computational region.

## COMPUTATIONAL METHOD

### Finite-Difference Equations

The computational region shown in figure 1 is divided with a polar grid system, and the flow properties are computed at the grid intersections at successive instants in time. The mesh spacings $\Delta r$, $\Delta\theta$, and $\Delta t$ are constants such that the ratios $\Delta t/\Delta r$ and $\Delta t/\Delta\theta$ do not exceed the limits specified by the Courant-Friedrichs-Lewy stability criteria, which are discussed later. The indices for the time $t$ and the coordinates $r$ and $\theta$ are $k$, $l$, and $m$, respectively.

The partial differential equations (1) to (7) are represented by the index equations

$$\frac{\partial A_i}{\partial t} + \frac{\partial B_i}{\partial r} + (1 + \nu)\frac{\partial C_i}{\partial \theta} + D_i + (1 - \nu)E_i \cot\theta = 0 \qquad (i = 1,2,3,4) \tag{8}$$

where

$$\left.\begin{aligned} \nu &= 1 \qquad (\theta = 0) \\ \nu &= 0 \qquad (\theta > 0) \end{aligned}\right\} \tag{9}$$

and where

$$\left.\begin{aligned}
&A_1 = \rho r \qquad A_2 = \rho u r \qquad A_3 = \rho v r \qquad A_4 = \left[\frac{1}{\gamma - 1}p + \frac{1}{2}\rho(u^2 + v^2)\right]r \\
&B_1 = \rho u r \qquad B_2 = (p + \rho u^2)r \qquad B_3 = \rho u v r \qquad B_4 = u\left[\frac{\gamma}{\gamma - 1}p + \frac{1}{2}\rho(u^2 + v^2)\right]r \\
&C_1 = \rho v \qquad C_2 = \rho u v \qquad C_3 = p + \rho v^2 \qquad C_4 = v\left[\frac{\gamma}{\gamma - 1}p + \frac{1}{2}\rho(u^2 + v^2)\right] \\
&D_1 = \rho u \qquad D_2 = -\left[p - \rho(u^2 - v^2)\right] \qquad D_3 = 2\rho u v \qquad D_4 = u\left[\frac{\gamma}{\gamma - 1}p + \frac{1}{2}\rho(u^2 + v^2)\right] \\
&E_1 = \rho v \qquad E_2 = \rho u v \qquad E_3 = \rho v^2 \qquad E_4 = v\left[\frac{\gamma}{\gamma - 1}p + \frac{1}{2}\rho(u^2 + v^2)\right]
\end{aligned}\right\} \tag{10}$$

The Lax technique can be extended to the problem which is being treated in this report by replacing the partial derivatives $(\partial A_i/\partial t)^k_{\ell,m}$ at the point $(k,\ell,m)$ with the forward difference expressions

$$\frac{(A_i)^{k+1}_{\ell,m} - \frac{1}{4}\left\{(A_i)^k_{\ell+1,m} + (A_i)^k_{\ell-1,m} + K\left[(A_i)^k_{\ell,m+1} + (A_i)^k_{\ell,m-1}\right]\right\}}{\Delta t}$$

where

$$\left.\begin{aligned} K &= 1 && (i = 1,4)\\ K &= \sec \Delta\theta && (i = 2,3)\end{aligned}\right\} \qquad (11)$$

and by using the central difference expressions

$$\frac{(B_i)^k_{\ell+1,m} - (B_i)^k_{\ell-1,m}}{2\,\Delta r}$$

and

$$\frac{(C_i)^k_{\ell,m+1} - (C_i)^k_{\ell,m-1}}{2\,\Delta\theta}$$

to represent the partial derivatives $(\partial B_i/\partial r)^k_{\ell,m}$ and $(\partial C_i/\partial\theta)^k_{\ell,m}$, respectively, at this point. The finite-difference expressions for the time derivatives in the momentum equations (i = 2,3) are modified so that they will vanish for uniform flow parallel to the axis. For uniform flow, $A_2$ and $A_3$ are not constant but vary as $\cos\theta$ and $\sin\theta$, respectively, and

$$(A_i)^k_{\ell,m+1} + (A_i)^k_{\ell,m-1} = 2(A_i)^k_{\ell,m}\cos\Delta\theta \qquad (i = 2,3)$$

If these sums were not modified, errors of order $(\Delta\theta)^2$ would be introduced into the solution for the uniform flow with each computation. The terms $(D_i)^k_{\ell,m}$ and $(E_i)^k_{\ell,m}$ at the point $(k,\ell,m)$ are replaced by the expressions

$$\frac{1}{4}\left[(D_i)^k_{l+1,m} + (D_i)^k_{l-1,m} + (D_i)^k_{l,m+1} + (D_i)^k_{l,m-1}\right]$$

and

$$\frac{1}{4}\left[(E_i)^k_{l+1,m} + (E_i)^k_{l-1,m} + (E_i)^k_{l,m+1} + (E_i)^k_{l,m-1}\right]$$

respectively.

The finite-difference expressions described above are used to obtain finite-difference representations for the partial differential equations (8) at the point $(k,l,m)$. They are written as

$$(A_i)^{k+1}_{l,m} = \frac{1}{4}\left\{(A_i)^k_{l+1,m} + (A_i)^k_{l-1,m} + \left[(A_i)^k_{l,m+1} + (A_i)^k_{l,m-1}\right]K\right\} + \frac{1}{2}\frac{\Delta t}{\Delta r}\left[(B_i)^k_{l-1,m} - (B_i)^k_{l+1,m}\right] + \frac{1}{2}\frac{\Delta t}{\Delta \theta}\left[(C_i)^k_{l,m-1} - (C_i)^k_{l,m+1}\right](1+\nu) - \frac{1}{4}\Delta t\left[(D_i)^k_{l+1,m} + (D_i)^k_{l-1,m} + (D_i)^k_{l,m+1} + (D_i)^k_{l,m-1}\right] - \frac{1}{4}\Delta t\left[(E_i)^k_{l+1,m} + (E_i)^k_{l-1,m} + (E_i)^k_{l,m+1} + (E_i)^k_{l,m-1}\right](1-\nu)\cot\theta \qquad (i = 1,2,3,4) \qquad (12)$$

All the quantities on the right-hand side of equations (12) have the time index $k$ and can be evaluated with the aid of equations (10) since the flow properties are known at time $k$.

Only the four points $(k, l+1, m)$, $(k, l-1, m)$, $(k, l, m+1)$, and $(k, l, m-1)$ are used to evaluate the right-hand side of equations (12); the point $(k,l,m)$ is not needed. Therefore, a staggered grid is used in this report, as shown in figure 2.

When the terms in equations (12) are replaced by Taylor series expansions about the point $(k,l,m)$, the following equations result:

$$\left(\frac{\partial A_i}{\partial t}\right)^k_{l,m} + \left(\frac{\partial B_i}{\partial r}\right)^k_{l,m} + (1+\nu)\left(\frac{\partial C_i}{\partial \theta}\right)^k_{l,m} + (D_i)^k_{l,m} + (1-\nu)(E_i)^k_{l,m}\cot\theta = -\frac{1}{2}\Delta t\left(\frac{\partial^2 A_i}{\partial t^2}\right)^k_{l,m} + \frac{1}{4}\frac{(\Delta r)^2}{\Delta t}\left(\frac{\partial^2 A_i}{\partial r^2}\right)^k_{l,m} + \frac{1}{4}\frac{(\Delta\theta)^2}{\Delta t}\left(\frac{\partial^2 A_i}{\partial \theta^2}\right)^k_{l,m} + \frac{1}{4}\frac{(\Delta\theta)^2}{\Delta t}(A_i)^k_{l,m}K_1 + 0(\Delta^2) \qquad (13)$$

$$(i = 1,2,3,4)$$

where

$$\left.\begin{aligned} K_l &= 0 \qquad (i = 1,4) \\ K_l &= 1 \qquad (i = 2,3) \end{aligned}\right\} \tag{14}$$

Equations (13) differ from equations (8) because of the presence of the terms on the right-hand side. Since the second and third terms are similar to some of the viscous terms in the viscous momentum equations, they are designated as "artificial viscosity" terms. The presence of these terms causes the inviscid flow properties to be continuous across shock waves. As a result, the shocks are smeared over several mesh spaces, and computations can be performed in their vicinity in the same manner as elsewhere. It can be shown that for uniform flow all the terms of order $\Delta$ on the right-hand side of equations (13) either vanish or cancel. The cancellation of terms in the momentum equations (i = 2,3) occurs because of the presence of the weighting function $K$ in the finite-difference equations (12).

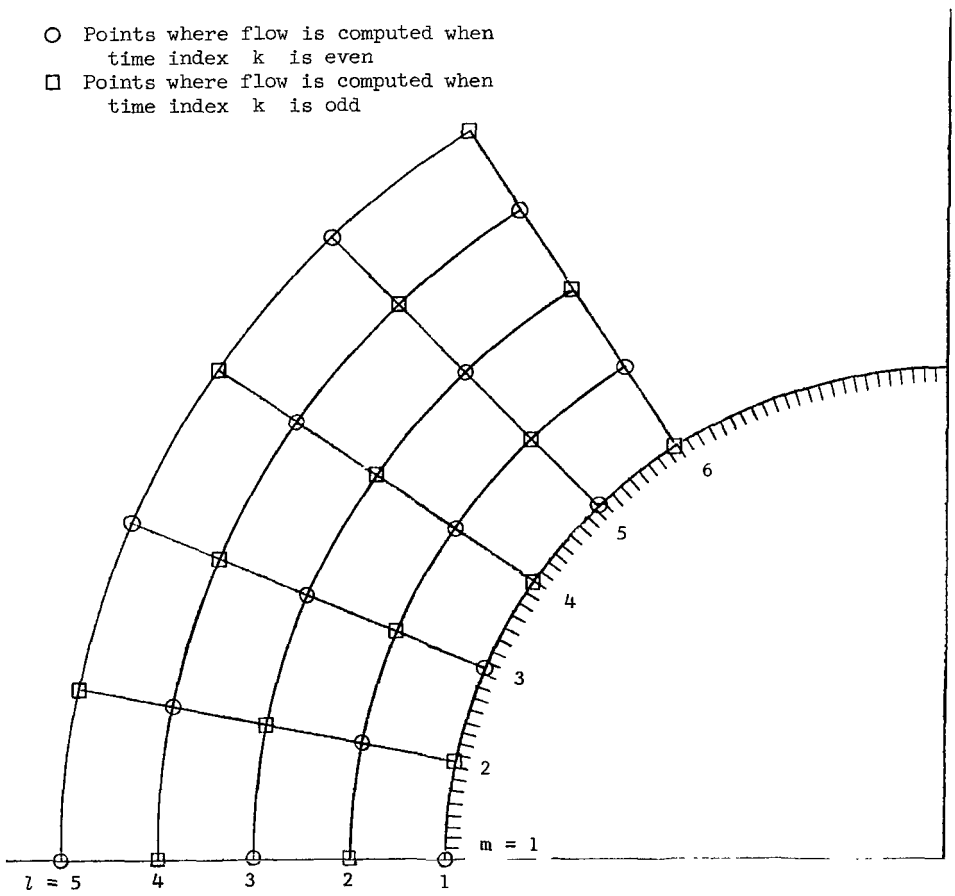


Figure 2.- Sample grid.

In this report equations (12) are used to determine the flow properties at points with an odd time index, and an alternate set of difference equations is used to obtain the flow properties at the points which have an even time index. This alternate set of equations does not contain implicit "artificial viscosity" terms. It has been found that the solutions which this alternating procedure yields are stable, and that the results are more accurate than those obtained when equations (12) are used exclusively.

The alternate set of finite-difference equations is obtained by replacing the quantities $(\partial A_i/\partial t)^k_{\ell,m}$, $(D_i)^k_{\ell,m}$, and $(E_i)^k_{\ell,m}$ at the point $(k,\ell,m)$ by the finite-difference expressions

$$\frac{(A_i)^{k+1}_{\ell,m} - \frac{1}{2}\left[(A_i)^k_{\ell+1,m} + (A_i)^k_{\ell-1,m}\right] + \frac{1}{8}\left[(A_i)^{k-1}_{\ell+2,m} - 2(A_i)^{k-1}_{\ell,m} + (A_i)^{k-1}_{\ell-2,m}\right]}{\Delta t}$$

$$\frac{1}{2}\left[(D_i)^k_{\ell+1,m} + (D_i)^k_{\ell-1,m}\right]$$

and

$$\frac{1}{2}\left[(E_i)^k_{\ell+1,m} + (E_i)^k_{\ell-1,m}\right]$$

respectively, and using the same expressions for the partial derivatives $(\partial B_i/\partial r)^k_{\ell,m}$ and $(\partial C_i/\partial \theta)^k_{\ell,m}$ as are used to obtain equations (12). When these expressions are substituted into equations (8), the following finite-difference equations result:

$$(A_i)^{k+1}_{\ell,m} = \frac{1}{2}\left[(A_i)^k_{\ell+1,m} + (A_i)^k_{\ell-1,m}\right] - \frac{1}{8}\left[(A_i)^{k-1}_{\ell+2,m} - 2(A_i)^{k-1}_{\ell,m} + (A_i)^{k-1}_{\ell-2,m}\right] + \frac{1}{2}\frac{\Delta t}{\Delta r}\left[(B_i)^k_{\ell-1,m} - (B_i)^k_{\ell+1,m}\right] + \frac{1+\nu}{2}\frac{\Delta t}{\Delta \theta}\left[(C_i)^k_{\ell,m-1} - (C_i)^k_{\ell,m+1}\right] - \frac{1}{2}\Delta t\left[(D_i)^k_{\ell+1,m} + (D_i)^k_{\ell-1,m}\right] - \frac{1-\nu}{2}\Delta t\left[(E_i)^k_{\ell+1,m} + (E_i)^k_{\ell-1,m}\right]\cot\theta \qquad (i = 1,2,3,4) \qquad (15)$$

Note that equations (15) are written for a staggered grid.

Results obtained by using equations (12) exclusively and by using equations (12) and (15) alternately are compared subsequently.

## Boundary Points

In order to compute the flow properties at a point on the axis ($\theta = 0$) with either equations (12) or (15), the flow properties for the previous time are required at points on either side of the axis. One of these points lies outside the region of computation. The flow properties at this outside point are evaluated by reflecting the properties at the corresponding point within the region of computation. The tangential velocity component $v$ is an odd function of $\theta$, and the other properties are even.

Equations (12) and (15) are used to determine the flow properties at points on the surface of the sphere as well as in the flow field. When these equations are used at the surface of the sphere or when equations (15) are used on the arc next to the surface, values are required for the flow properties at fictitious points which are located within the sphere. These values are obtained by reflecting the values at the points which lie an equal distance outside the surface along the same radial line. The radial velocity component $u$ is treated as an odd function, and the other flow properties are considered to be even functions. One consequence of this procedure is that the finite-difference expressions which represent the normal derivatives $(\partial B_i/\partial r)_{r=r_b}$ $(i = 1,3,4)$ at the body vanish. This is not physically correct, but it is tolerated since it does not cause appreciable error. The radial momentum equation ($i = 2$) is not used at the surface since the radial component $u$ is known to be zero when $r = r_b$.

The flow properties at points along the arc $r = r_{max}$ are those of either the undisturbed gas or the uniform flow behind the incident shock wave. During the early part of the computation when the incident shock wave intersects this arc, the location of the intersection is determined from the incident-shock speed and the field of computation, and the flow properties at points on the arc are assigned accordingly. Uniform flow properties are maintained along the arc when the incident shock no longer intersects it.

The incident shock wave is advanced along the line $\theta = \theta_{max}$ in a manner similar to that which is used for the arc $r = r_{max}$. When the incident shock wave has passed out of the computational region, the flow properties along the line $\theta = \theta_{max}$ are determined by extrapolating the quantities $C_i$ linearly. The line $\theta = \theta_{max}$ is located in a region where the flow is supersonic at all times after the incident shock wave has passed, because the extrapolation procedure is not stable if the flow is locally subsonic.

## Stability Criteria

The Courant-Friedrichs-Lewy stability conditions (ref. 15) for the partial differential equations which govern inviscid, compressible fluid flow place an upper bound on the mesh spacing $\Delta t$ for particular values of the other mesh spacings. These conditions for a spherical polar coordinate system are

$$\frac{\Delta t}{\Delta r} \leq \frac{1}{|u| + a} \qquad \frac{\Delta t}{\Delta \theta} \leq \frac{r}{|v| + a} \tag{16}$$

If these conditions are not met the solution at time $k + 1$ will not be influenced properly by the solution at previous times and unstable computations can result. The present research indicates that these stability conditions, with the limitation mentioned below, are sufficient.

Since the mesh spacings are constant for a given computation, the smallest values of the terms on the right-hand side of the inequalities (16) must be used. According to exact calculations, the smallest value for the right-hand side of the inequality for $\Delta t/\Delta r$ for the cases treated is $(V_\infty + a_\infty)^{-1}$. However, it was found that the use of this value led to instabilities during the period of shock reflection. These instabilities occurred because the shock waves are smeared over several mesh spaces, and the flow properties are mixed within the smeared shock. The instabilities can be removed by using the speed of sound behind the reflected shock immediately after the shock impingement in the stability criterion instead of $a_\infty$.

# RESULTS

The numerical method presented in this report is used to investigate the diffraction of a normal shock wave by a sphere and the subsequent transient phenomena in an inviscid, perfect-gas flow field. The transient behavior in the region ahead of the sphere is studied for ranges of the incident-shock Mach number $M_S$ and the specific-heat ratio $\gamma$. Time histories are presented for the shock detachment distance and the stagnation-point pressure and tangential velocity gradient in terms of the nondimensional time parameter

$$\tau = \frac{ct}{\delta_S} \tag{17}$$

where $t$ is the time after shock impingement, $c$ is the speed of the reflected shock in the corresponding one-dimensional shock reflection problem, and $\delta_S$ is the shock detachment distance for steady flow.

The flow field under consideration has three regions: the undisturbed region ahead of the incident shock, the region of uniform flow behind the incident shock, and the shock layer between the reflected shock wave and the body.

The local Mach number in the region of uniform flow behind the incident shock is related to $\gamma$ and $M_S$ by the equation

$$M_\infty{}^2 = \frac{2}{\gamma(\gamma - 1)} \frac{\left(1 - \frac{1}{M_S{}^2}\right)^2}{\left(1 - \frac{\gamma - 1}{2\gamma}\frac{1}{M_S{}^2}\right)\left(1 + \frac{2}{\gamma - 1}\frac{1}{M_S{}^2}\right)}$$

Thus, $M_\infty$ has a limiting value as $M_S \to \infty$ for each value of $\gamma$. This limiting value is finite for $\gamma > 1$.

Lighthill (ref. 16) generalizes the one-dimensional shock reflection problem in order to treat shock reflection at a plane surface which is slightly inclined to the incident shock wave. To the first order in the angle of inclination $\theta$ the expressions for the speed of the reflected shock wave and the thermodynamic properties behind the reflected shock are the same as those for the one-dimensional shock reflection problem. The expression for the velocity component tangent to the plane surface behind the reflected shock is

$$v = V_\infty \frac{3\gamma - 1}{\gamma + 1}\left(1 + \frac{3 - \gamma}{3\gamma - 1}\frac{1}{M_S{}^2}\right)\theta \tag{18}$$

This expression may be used to evaluate the tangential velocity component at the point where a normal shock wave is reflected by a sphere for the period immediately after shock impingement.

## Detailed Time-History Calculations

The diffraction of the incident shock wave by the sphere and the subsequent motion of the reflected shock wave for $\gamma = 1.4$ and $M_S = 5.55$ ($M_\infty = 1.70$) are shown in figure 3. The shock waves shown in the figures are positioned at the midpoints of the rapid rises in the pressure profiles across the shocks. The computation is initiated at $\tau = -0.21$ before shock impingement has occurred. The shock wave moves downstream, strikes the sphere, and is reflected. Initially, the reflection is regular. When the angle of inclination of the incident shock to the surface has increased, Mach reflection occurs. Examples of regular and Mach reflection are shown in figure 3(a) for $\tau = 0.088$ and $\tau = 0.37$, respectively.

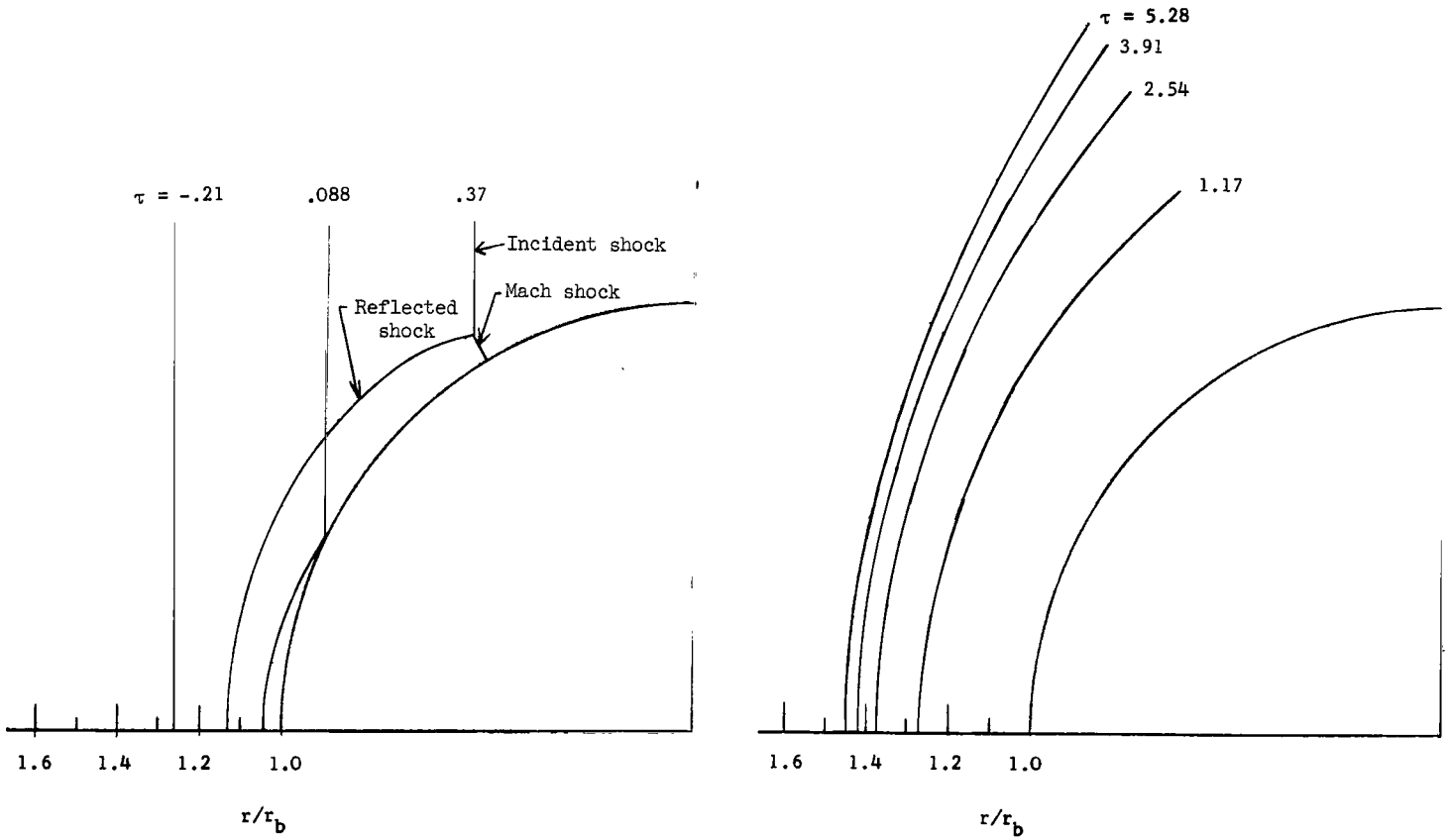


(a) Normal shock striking sphere.

(b) Subsequent transient motion.

Figure 3.- Diffraction of normal shock wave by sphere for $\gamma = 1.4$ and $M_s = 5.55$ $(M_\infty = 1.70)$.

This change from regular to Mach reflection is similar to the change which occurs in the inclined-plane shock reflection problem. It is shown in reference 17 that the angle of inclination of the shock wave to the plane surface has an upper bound above which regular reflection is not possible, and a lower bound below which Mach reflection cannot occur. These bounds are functions of $\gamma$ and $M_S$, and they do not coincide; there is an overlap region where both types of reflection are mathematically possible.

The present method does not determine the angle of inclination at which Mach reflection is initiated in the shock wave-sphere interaction problem. Bryson and Gross (ref. 6) show that the length of the Mach shock is a very small fraction of the radius of the sphere for some time after Mach reflection begins. The Mach shock is defined clearly by the present method only after its length is greater than the radial mesh spacing $\Delta r$.

The computational method must be modified in order to make calculations in the vicinity of the Mach shock, because the alternate use of equations (12) and (15) does not yield stable solutions at the Mach shock. For this reason, equations (12) are used exclusively at the points in $(r, \theta, t)$ space where Mach reflection can occur. When the Mach shock has moved out of the computational region, the alternating procedure is used throughout the flow field.

In figure 4 the shock and sonic-line locations for $\tau = 5.28$ are compared with the experimental results of Ladenburg, Winckler, and Van Voorhis (ref. 18) for the steady flow of air over a sphere at $M_\infty = 1.70$. The numerical results for the shock-wave location for $\tau = 5.28$ and the experimental results are in agreement near the axis where the numerical solution has reached the steady state. The numerical solution is still slightly transient at points away from the axis and in the vicinity of the shock wave. The numerical solution for the sonic line has the same general character as the experimental results. A firm conclusion cannot be drawn because of the scatter in the experimental points. The numerical solution does not extend to the shock wave because of the smearing of the flow properties in the vicinity of the shock.

The transient stagnation streamline distributions of several of the flow properties for $\gamma = 1.4$ and $M_S = 5.55$ are shown in figures 5, 6, 7, and 8. These distributions are obtained by alternately using equations (12) and (15). Those obtained by exclusive use of equations (12) are compared with the results of the present method for $\tau = 5.28$ when the flow along the stagnation streamline has become steady.

In figure 5 the transient pressure distributions are shown. The pressure drops rapidly after the initial overpressure so that the pressure profile within the layer approaches its steady configuration before the shock detachment distance attains its steady value. The pressure profile at $\tau = 0.12$ shows the maximum value of the stagnation-point pressure that is encountered during the computation. It is seen in the

figure that the maximum overpressure compares closely with the pressure behind the reflected shock in the one-dimensional shock reflection problem. The time $\tau = 0$ corresponds to the time at which the incident shock should reach the body according to an exact one-dimensional shock computation. The numerically determined overpressure occurs a little later because the incident and reflected shock waves are smeared over several mesh spaces, and it takes several time steps for the reflection to occur.

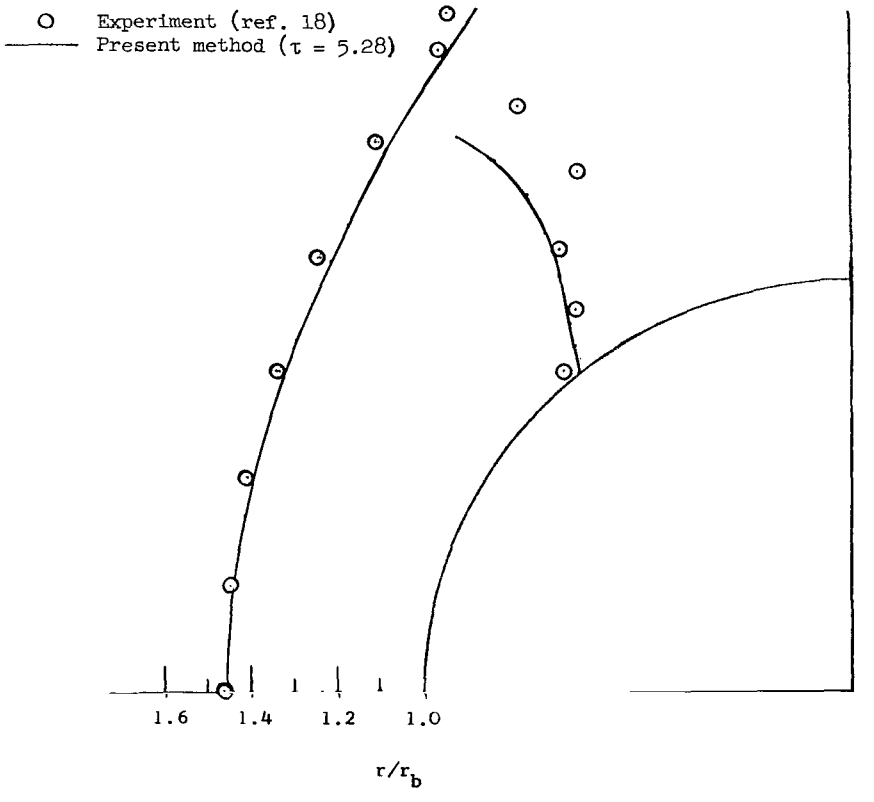


Figure 4.- Steady shock-wave and sonic-line locations for $\gamma = 1.4$ and $M_s = 5.55$ $(M_\infty = 1.70)$.

It is seen in figure 6 that the variation of the density profile with time is similar to that of the pressure profile. The maximum value of the numerically computed stagnation-point density occurs at the same time that the maximum overpressure occurs. The present method computes pressure more accurately than density. The numerically computed steady stagnation-point values for pressure and density are within 1 percent and 5 percent of their respective exact values.

The distribution of the tangential velocity gradient for several times is shown in figure 7. It is seen that the numerical solution for the stagnation-point gradient attains

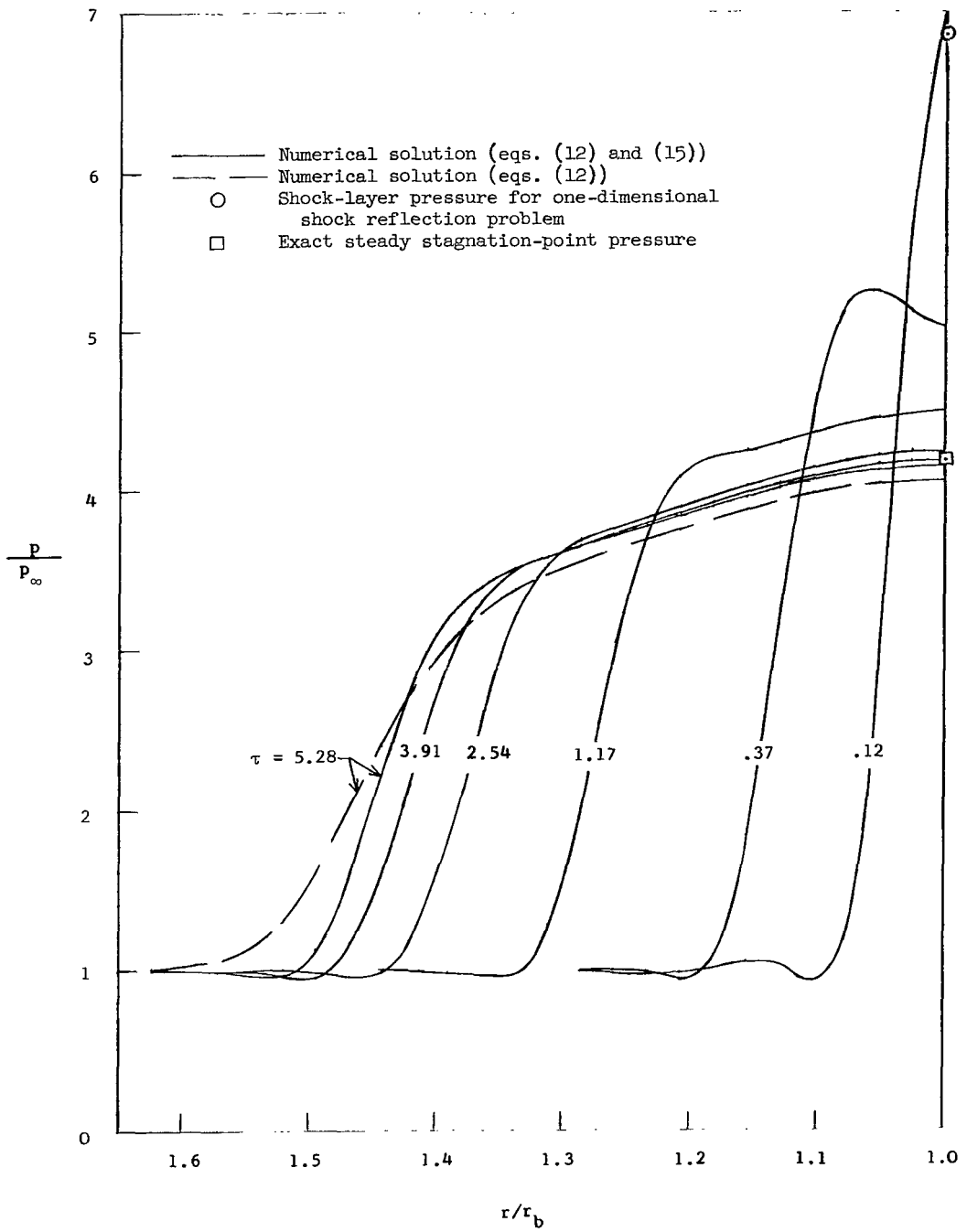


Figure 5.- Transient stagnation streamline pressure distributions for $\gamma = 1.4$ and $M_s = 5.55$ $(M_\infty = 1.70)$.

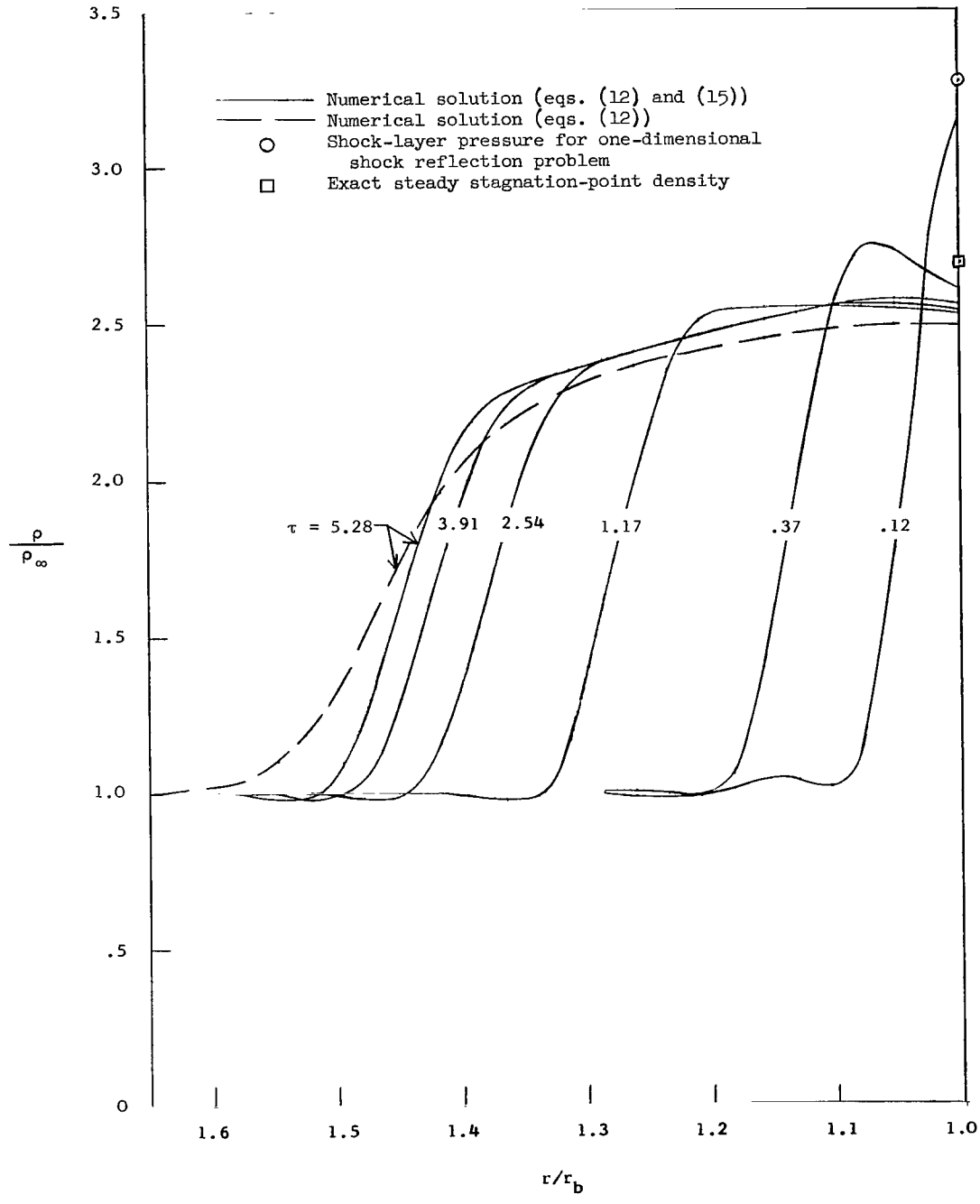


Figure 6.- Transient stagnation streamline density distribution for $\gamma = 1.4$ and $M_s = 5.55$ $(M_\infty = 1.70)$.

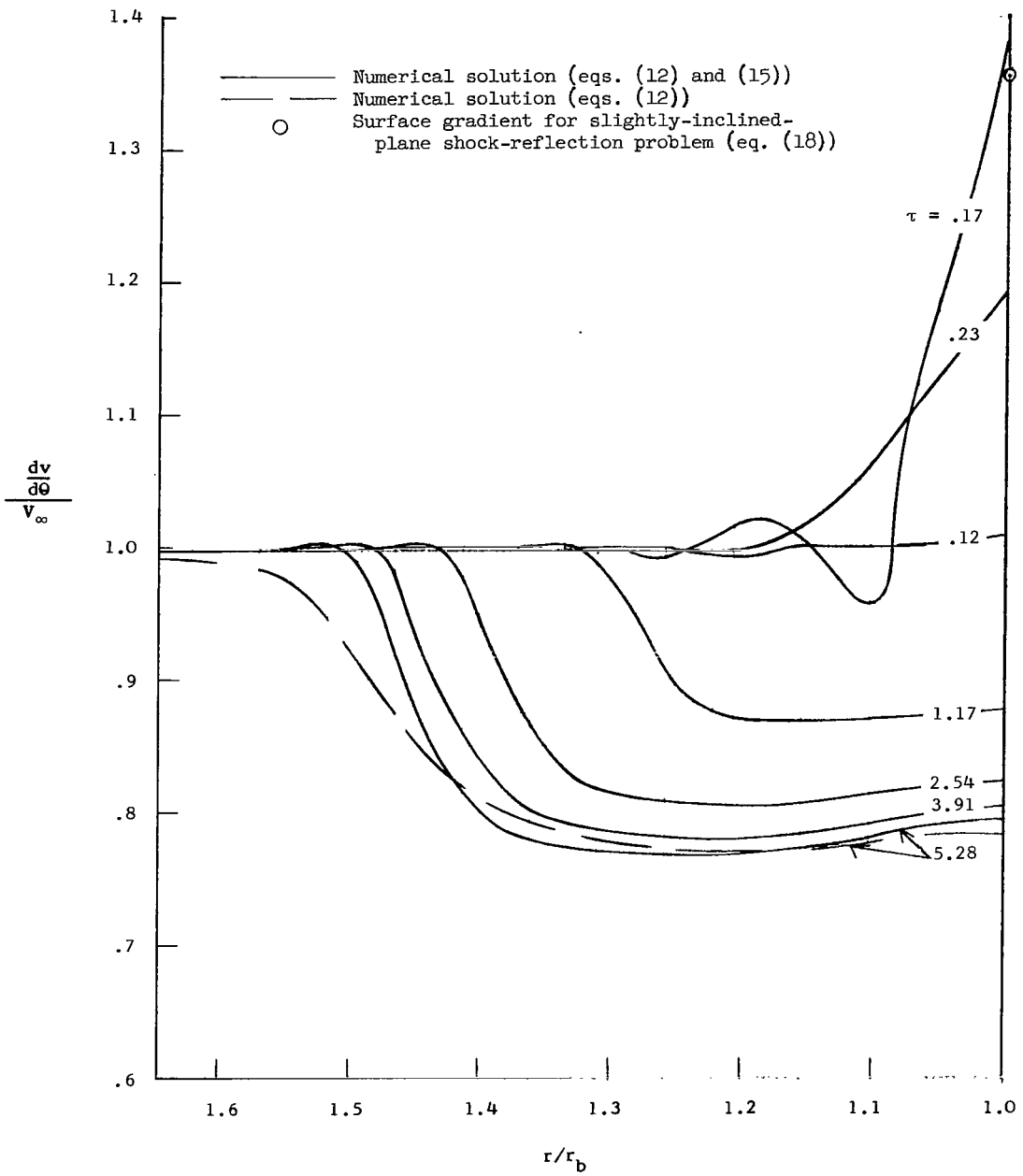


Figure 7.- Transient stagnation streamline tangential-velocity-gradient distributions for $\gamma = 1.4$ and $M_s = 5.55$ $(M_\infty = 1.70)$.

its maximum value after the maximum overpressure occurs. This maximum value is close to the value given by equation (18). The tangential velocity gradients along the axis drop rapidly from the peak values and then approach the steady values slowly.

In figure 8 it is seen that the local Mach numbers at points along the stagnation streamline within the shock layer adjust to their steady values even more rapidly than the other flow properties do. This phenomenon was observed for all the cases treated.

The steady distributions which are obtained by using equations (12) exclusively are seen to be less accurate than those of the present method. The stagnation-point thermodynamic properties are more in error, and the profiles are smeared more at the shock wave. It should be noted that the mesh spacings which are used for the two computations are identical; only the methods of computation differ.

In figure 9 the numerical results for the steady pressure distribution along the surface of the sphere for the case $\gamma = 1.4$ and $M_S = 30$ ($M_\infty = 1.88$) are compared with the experimental results of Kendall (ref. 19) for a sphere in air with $M_\infty = 1.82$. Kendall reports that his pressure measurements are accurate to within 1 percent and that viscous effects do not influence his results. Also, in figure 9 the numerical surface Mach number distribution is compared with the one given in reference 19. The results of the present method are seen to be in good agreement with the results of Kendall.

## Shock-Detachment-Distance Histories

Numerical results for the transient behavior of the shock detachment distance for several cases are presented in figure 10. The nondimensional quantity $\delta/\delta_S$ is plotted against $\tau$, where the values for steady shock detachment distance $\delta_S$ are determined from the results of Van Dyke and Gordon (ref. 20) and Lomax and Inouye (ref. 21). The cases for $\gamma = 1.1$ and $\gamma = 1.4$ span a wide range of the incident shock Mach number $M_S$. As $M_\infty$ approaches unity the shock layer becomes large and difficult to compute when the steady state is approached. For this reason, the case $\gamma = 1.4$ and $M_S = 2.51$ ($M_\infty = 1.20$) is terminated before steady flow is established. Since $M_\infty$ is small for all values of $M_S$ when $\gamma$ is large, only one case is presented for $\gamma = 5/3$.

It can be seen from figure 10 that the shock-detachment-distance histories are not very sensitive to mesh spacing size. In this figure results are presented for two computations for each of the cases $\gamma = 1.1$ and $M_S = \infty$ ($M_\infty = 4.26$) and $\gamma = 5/3$ and $M_S = \infty$ ($M_\infty = 1.34$). Finer mesh spacings were used for the computations indicated by the solid symbols.

All the data points in figure 10 lie in a fairly narrow band. This result indicates that the nondimensional time $\tau$ is an effective scaling parameter. In general, the data points are arranged within the band according to the value of $M_\infty$.

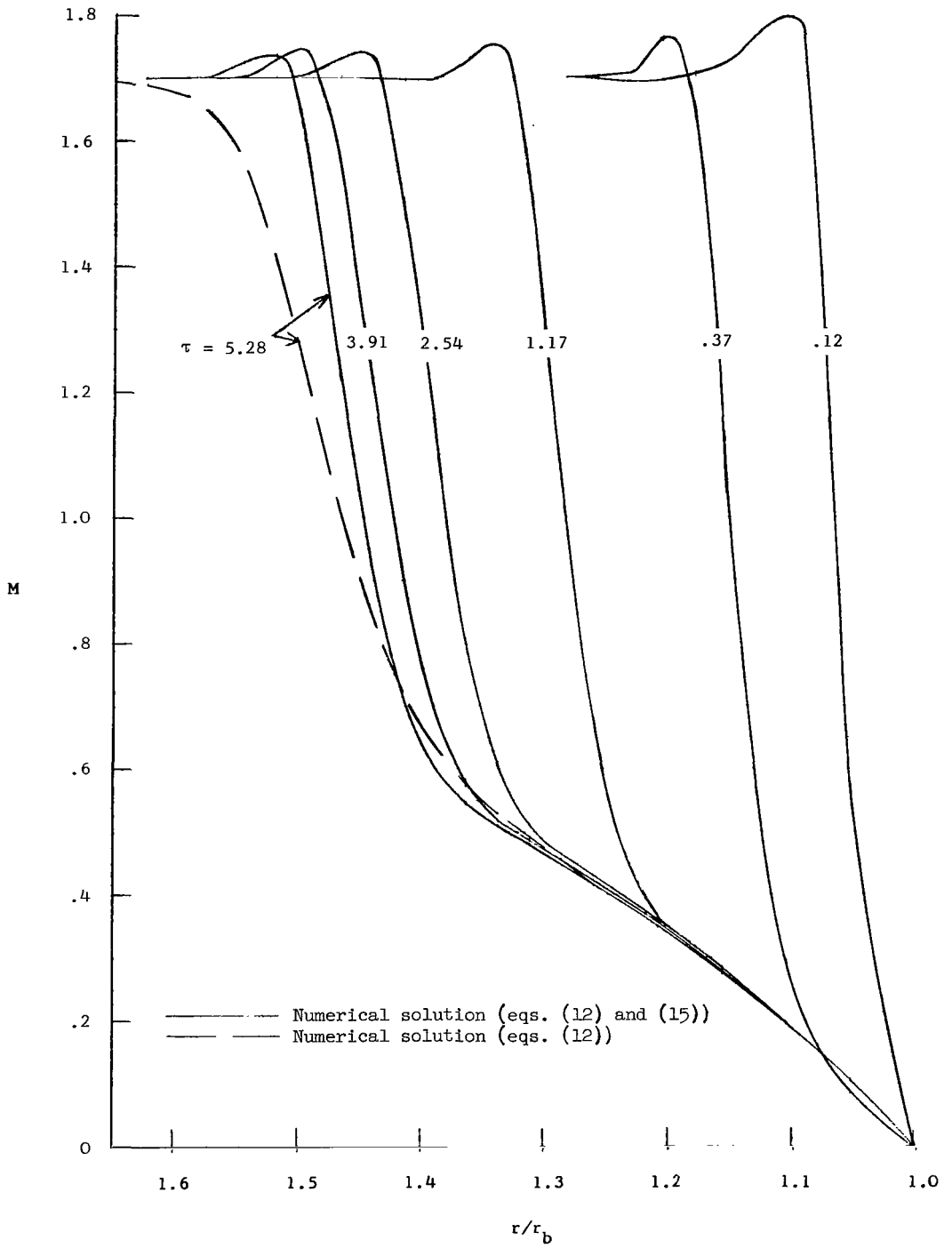


Figure 8.- Transient stagnation streamline Mach number distributions for $\gamma = 1.4$ and $M_s = 5.55$ $(M_\infty = 1.70)$.

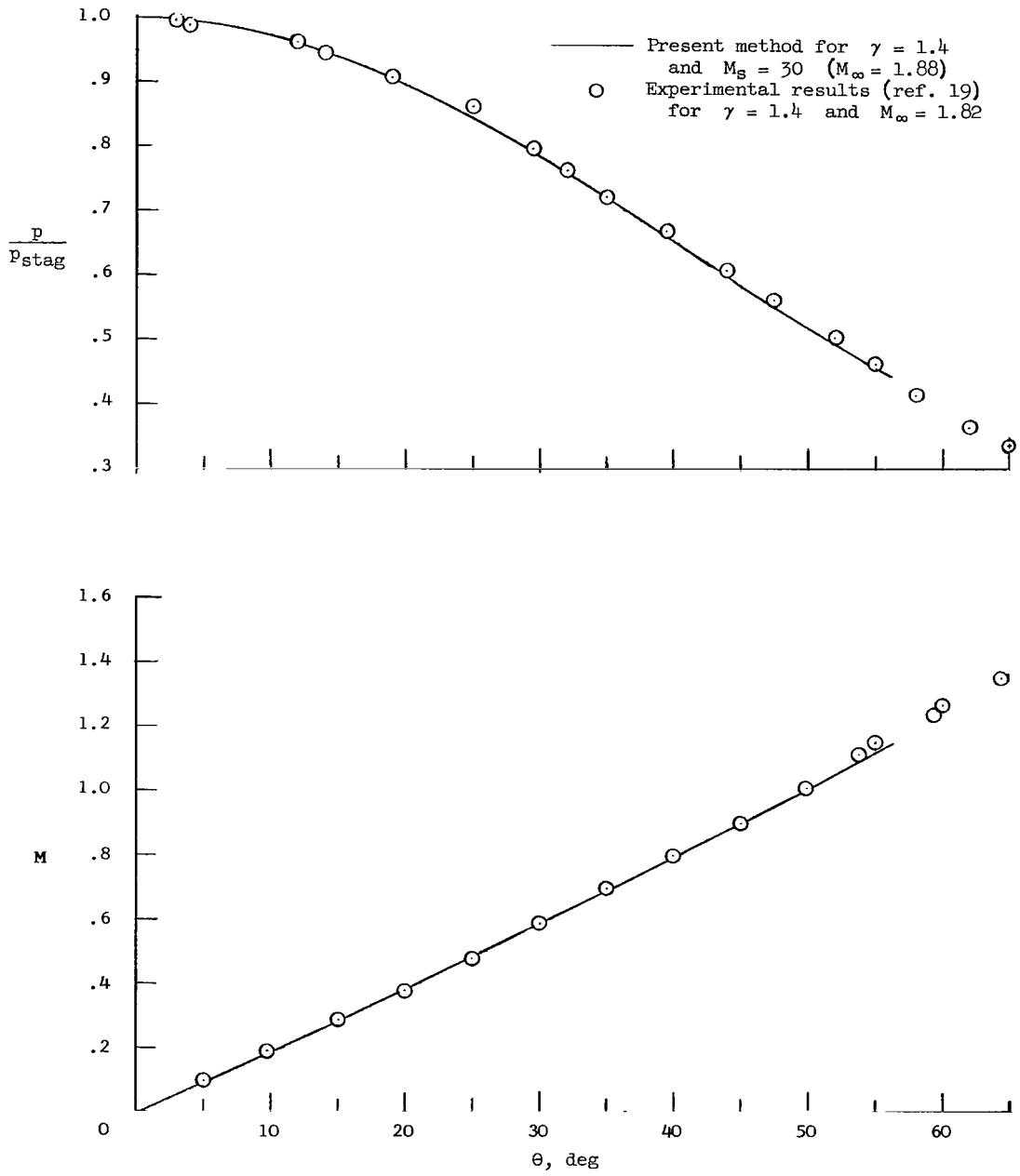


Figure 9.- Steady surface-pressure and Mach number distributions.

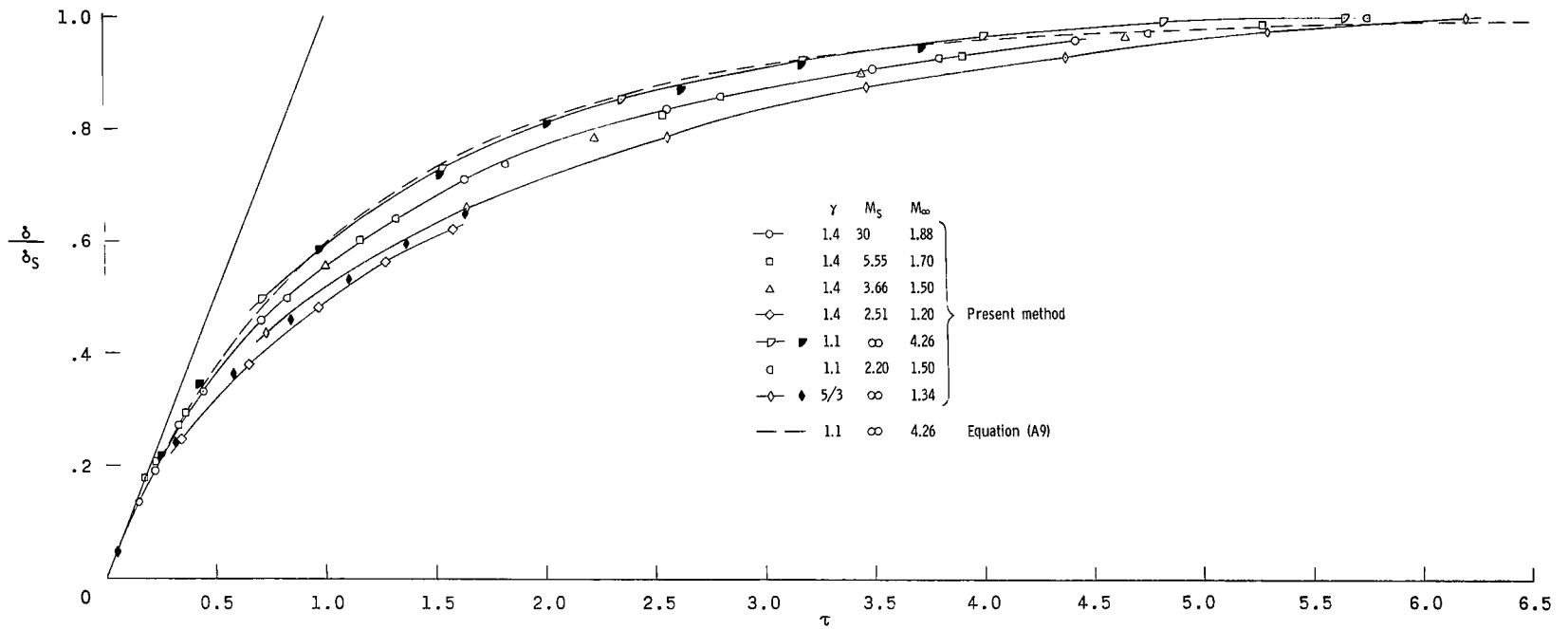


Figure 10.- Shock detachment histories.

Several cases are treated for $\gamma = 1.4$ to determine the asymptotic behavior of the shock-detachment-distance histories as $M_S$ is increased. It is seen in the figure that the histories approach the limiting case for fairly low values of $M_S$; the data points for $M_S = 30$, 5.55, and 3.66 lie very near the same curve in the figure.

An approximate analytical solution for the variation of the shock detachment distance with time is obtained in the appendix for cases with values of $\gamma$ near unity and large values of $M_S$. This solution for $\gamma = 1.1$ and $M_S = \infty$ ($M_\infty = 4.26$) is shown in figure 10. The constant $\alpha$ is evaluated by using the exact steady values of 10.00 and 10.49 for the density ratios $\overline{\rho}_{S,S}$ and $\overline{\rho}_{b,S}$, respectively; the numerically obtained value of 0.615 for $\overline{v}'_{b,S}$, the steady nondimensional tangential velocity gradient at the body; and the approximate value of 1 for $\overline{v}'_S$, the nondimensional tangential velocity gradient at the shock. It is seen in the figure that the analytical solution and the numerical solution are in good agreement. Equation (A6) yields a value of 0.067 for $\overline{\delta}_S$, as opposed to the numerically obtained value of 0.080.

## Stagnation-Point-Pressure Histories

The numerical results for the stagnation-point-pressure histories are presented in figure 11. The nondimensional pressure $p_{stag}/p_\infty$ is plotted against $\tau$. Initially, an overpressure occurs at the stagnation point. Then the pressure drops rapidly and approaches its steady value monotonically. The results of Butler (ref. 9) show that the transient stagnation-point pressure for a flat-nosed cylinder undershoots the steady value when $\gamma$ is low and $M_S$ is high. This phenomenon is not observed in the present results for the sphere. The maximum overpressures which are observed are in fair agreement with the pressures behind the reflected shock in the one-dimensional reflected shock problem, as mentioned earlier. The numerical results for the steady values are in good agreement with the exact values.

A comparison of the results in figures 10 and 11 shows that the stagnation-point pressure approaches its steady value much more rapidly than the shock detachment distance does. The pressures are within about 5 percent of the final values at $\tau = 1.5$. At this time the shock detachment distances have reached only about 70 percent of their final values. The shock detachment distances approach the final values at $\tau = 5$ or 6. The asymptotic behavior of the stagnation-point densities and temperatures is similar to that of the pressures.

The initial overpressures are very sensitive to the stability criterion and the size of the mesh spacings. If the stability criterion is exceeded, the computations within the shock layer immediately after shock impingement are erratic. If the mesh spacing is crude, the peak values are not obtained although the solution at later times is not affected appreciably. This sensitivity to mesh spacing is more pronounced for low values of $\gamma$.

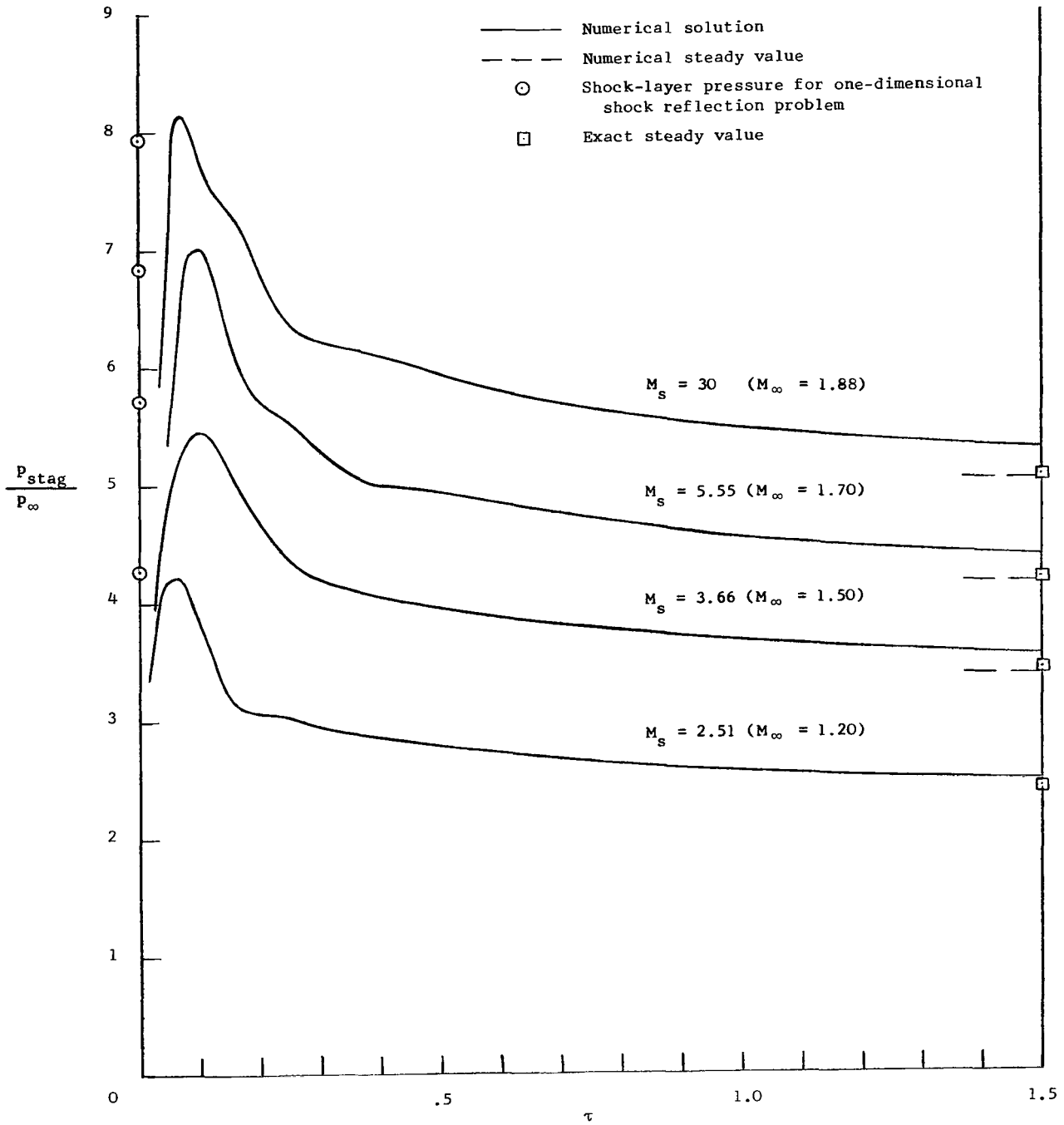


(a) $\gamma$ = 1.4.

Figure 11.- Stagnation-point pressure histories.

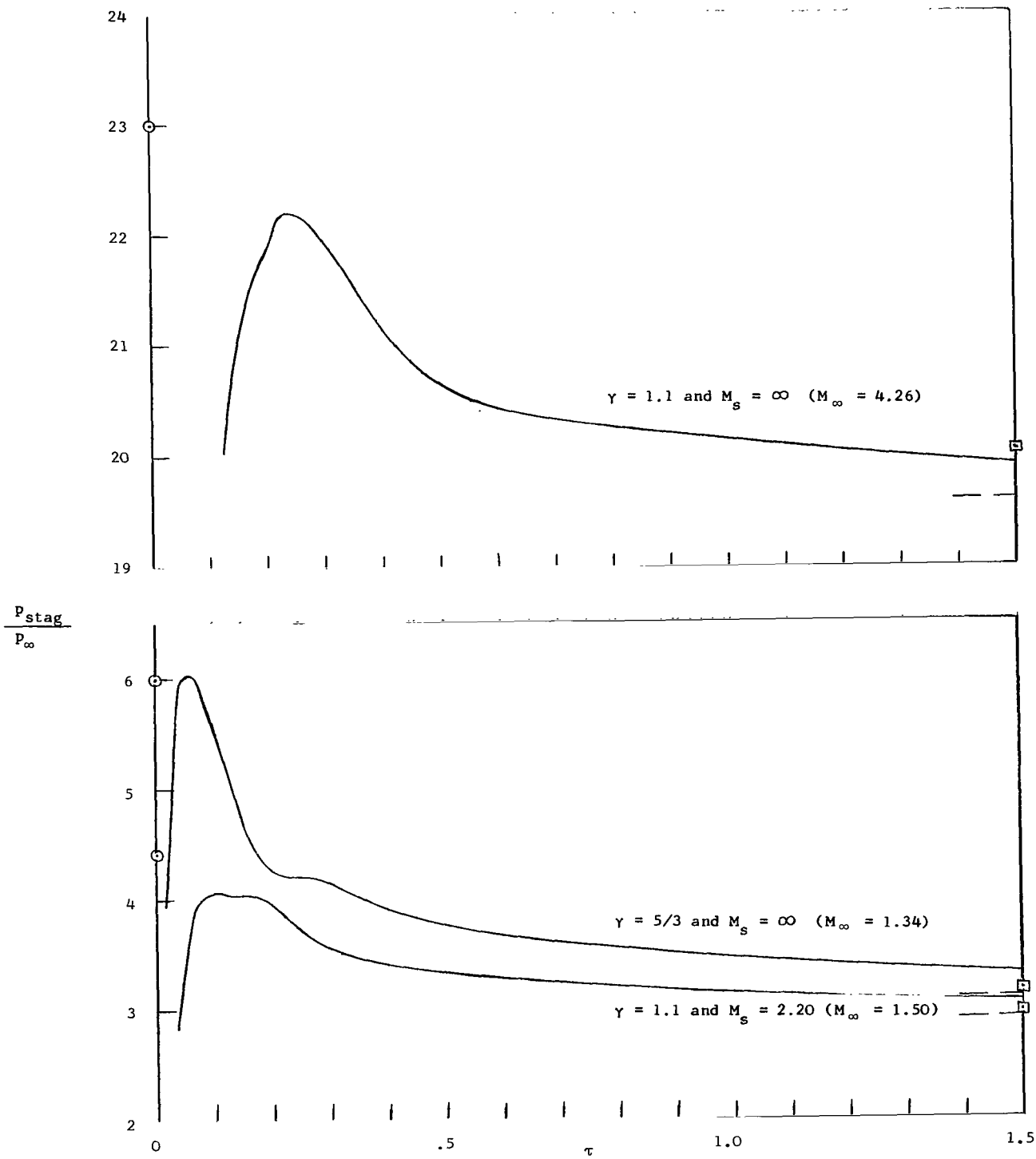


(b) $\gamma = 1.1$ and $\gamma = 5/3$.

Figure 11.- Concluded.

### Stagnation-Point Tangential-Velocity-Gradient Histories

The numerical results for the stagnation-point tangential-velocity-gradient histories are presented in figure 12. The nondimensional quantity $\frac{1}{V_\infty}\left(\frac{dv}{d\theta}\right)_{stag}$ is plotted against $\tau$. It is seen in the figure that the initial velocity gradient is larger than the steady value. After shock impingement the stagnation-point velocity gradient approaches the steady value monotonically. In figure 13 the stagnation-point tangential velocity gradient is plotted against the shock detachment distance. The velocity gradient is nondimensionalized with the value which is obtained by differentiating equation (18) with respect to $\theta$, and the shock detachment is nondimensionalized with its steady value. For the cases shown the variation of the velocity gradient with the shock detachment distance becomes more nearly linear as $M_\infty$ is increased, and the steady gradients are approximately 60 percent of the values given by equation (18). These observations hold for all the cases which were treated.

Results for two computations with different mesh spacings are shown in figures 12 and 13. Finer mesh spacings were used for the computations indicated by the solid symbols. It is seen that the stagnation-point velocity-gradient histories are fairly insensitive to mesh spacing.

## CONCLUDING REMARKS

Numerical results are presented for the unsteady flow in the shock layer of a sphere which has been washed by a normal shock wave. The numerical values for the overpressure in the shock layer immediately after shock impingement are in good agreement with the exact calculations for the pressure behind the reflected shock in the corresponding one-dimensional shock-reflection problem. The results show that the growth of the shock-layer thickness is much slower than the adjustment of the stagnation-point thermodynamic properties to their steady values. This means that the stagnation-point pressure is not a good indicator of steady flow. The stagnation-point tangential velocity gradient also approaches its steady value faster than the shock-layer thickness for all but the largest free-stream Mach number.

It is shown that the histories of the nondimensional shock detachment distance $\delta/\delta_S$ (where $\delta_S$ is the steady shock detachment distance) can be scaled effectively with the nondimensional time $\tau = ct/\delta_S$ (where $c$ is the initial reflected-shock speed and $t$ is the time after shock impingement). The ratio $\delta/\delta_S$ approaches 1 for values of $\tau$ of about 5 or 6 for a wide range of perfect-gas specific heat ratio $\gamma$ and incident-shock-wave Mach number $M_S$. Therefore, an estimate of the time necessary to establish steady flow can be obtained if estimates of $\delta_S$ and $c$ are available.

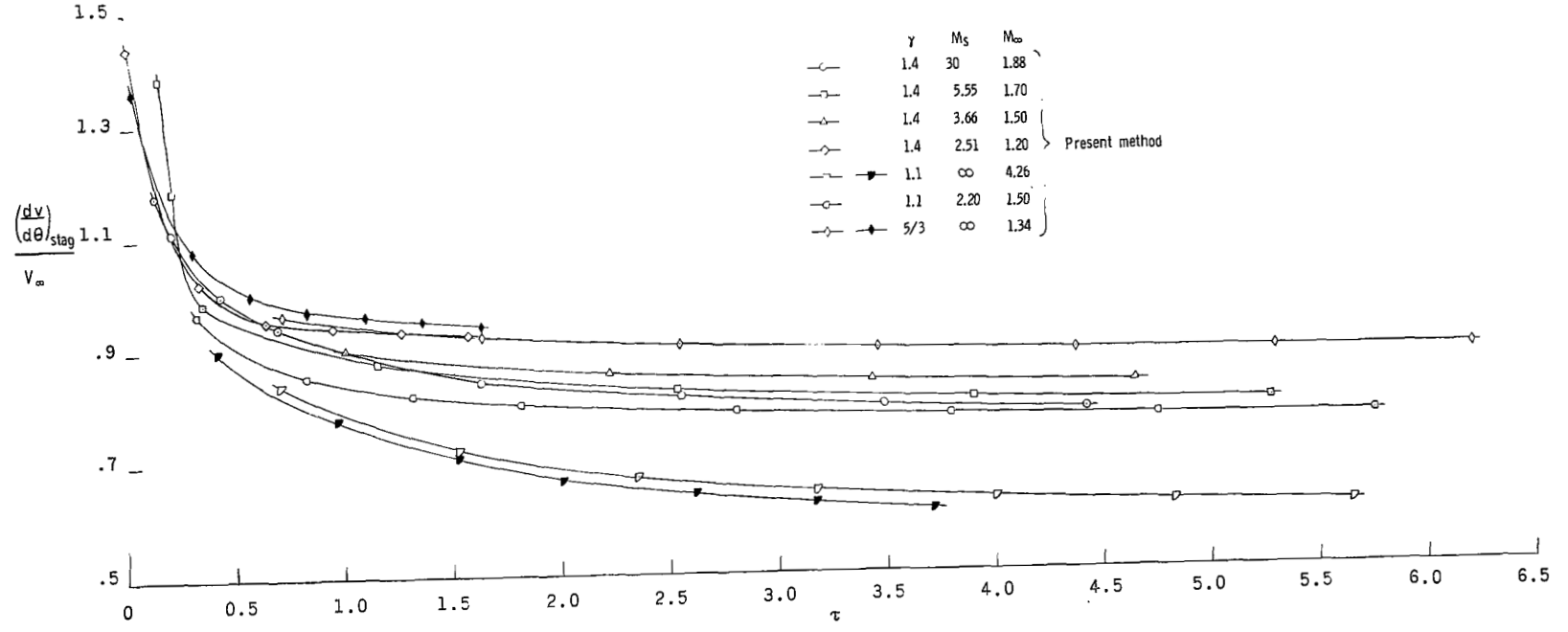


Figure 12.- Stagnation-point tangential-velocity-gradient histories.

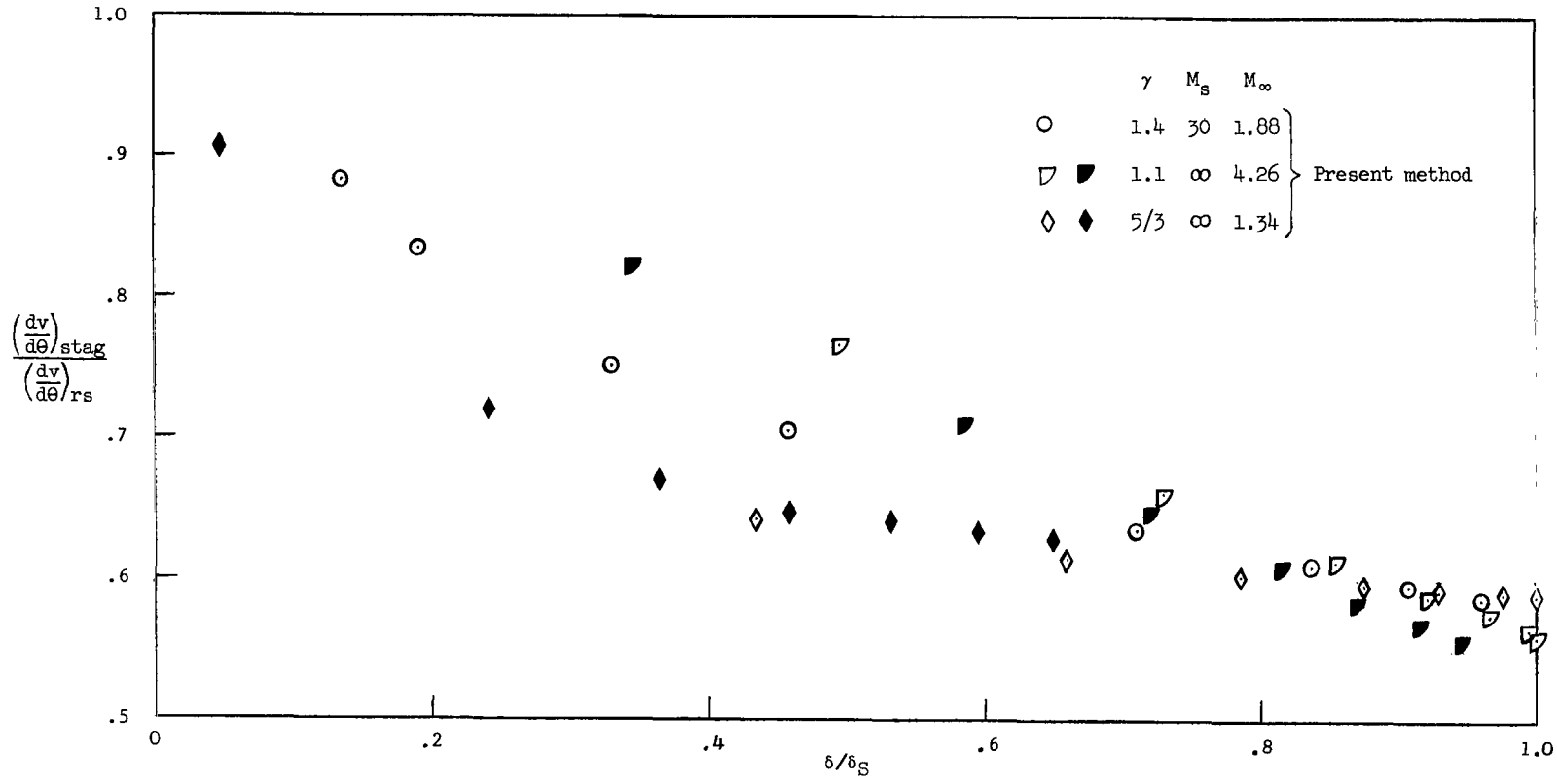


Figure 13.- Stagnation-point tangential velocity gradient as a function of shock detachment.

An approximate analytical solution is obtained for the shock-detachment-distance histories for cases with large values of $M_s$ and values of $\gamma$ near unity.

Langley Research Center,
National Aeronautics and Space Administration,
Langley Station, Hampton, Va., January 25, 1967,
129-01-08-18-23.

## APPENDIX

## APPROXIMATE EXPRESSION FOR TIME HISTORY OF SHOCK DETACHMENT DISTANCE

A simple analytical expression can be obtained for the time variation of shock detachment distance for cases with values of $\gamma$ near unity and large values of $M_s$. Under these conditions $M_\infty$ will be large, and the shock layer will be close to the body and can be approximated by a spherical cap in the stagnation region. In addition, the initial overshoots in the stagnation region are small for these conditions.

When the reflected shock wave is approximated by a spherical surface, the tangential velocity gradient immediately behind the shock is approximated by the free-stream gradient $dv/d\theta = V_\infty \cos\theta$. This gradient along the axis is simply $V_\infty$. It should be noted that this approximation is good for the period immediately following shock impingement since the gradient given in equation (18) approaches $V_\infty$ for small $\gamma$ and large $M_s$.

The tangential velocity component in the vicinity of the axis is assumed to be of the form $v = v'\theta$, where the prime denotes differentiation with respect to $\theta$. The thermodynamic properties, u, and v' are assumed to be functions of r and t near the axis.

The one-strip method of integral relations of Belotserkovskii (ref. 22) is used to integrate equation (5), the continuity equation for flow along the axis, across the shock layer. The general form for the integrated equation is

$$\int_{r=r_b}^{r=r_b+\delta} \frac{\partial(\rho r)}{\partial t}\,dr + \rho_s u_s\left(r_b + \delta\right) + 2\int_{r=r_b}^{r=r_b+\delta} \rho v'\,dr + \int_{r=r_b}^{r=r_b+\delta} \rho u\,dr = 0$$

The quantities $\rho r$, $\rho v'$, and $\rho u$ in this equation are approximated with linear profiles across the shock layer. The integrated equation is written as

$$\frac{\delta}{2}\left[r_b \frac{d\rho_b}{dt} + \left(r_b + \delta\right)\frac{d\rho_s}{dt}\right] + \frac{r_b}{2}\left(\rho_b - \rho_s\right)\frac{d\delta}{dt} + \rho_s u_s\left(r_b + \frac{3}{2}\,\delta\right) + \delta\left(\rho_b v_b' + \rho_s v_s'\right) = 0 \qquad \text{(A1)}$$

The shock relation

$$\rho_s\left(u_s - \frac{d\delta}{dt}\right) = \rho_\infty\left(u_\infty - \frac{d\delta}{dt}\right) \qquad \text{(A2)}$$

is used to evaluate the term $\rho_s u_s$. The tangential velocity gradient at the body is assumed to vary linearly with $\delta/\delta_S$. This assumption is made because $M_\infty$ is large when $M_S$ is large and $\gamma$ is near unity, and the variation of the velocity gradient with the shock detachment distance becomes more nearly linear as $M_\infty$ is increased, as shown in figure 13. The expression for $v'_b$ is written as

$$v'_b = v'_s - \left(v'_s - v'_{b,S}\right)\frac{\delta}{\delta_S} \tag{A3}$$

The quantities in equations (A1), (A2), and (A3) are nondimensionalized as follows (the barred quantities are nondimensional):

$$\bar{u} = \frac{u}{V_\infty} \qquad \bar{v}' = \frac{v'}{V_\infty} \qquad \bar{\rho} = \frac{\rho}{\rho_\infty} \qquad \bar{\delta} = \frac{\delta}{r_b} \qquad \bar{t} = \frac{t}{r_b/V_\infty} \tag{A4}$$

where $u_\infty = -V_\infty$. The equation is written as

$$\frac{\bar{\delta}}{2}\left[\frac{d\bar{\rho}_b}{d\bar{t}} + \left(1 + \bar{\delta}\right)\frac{d\bar{\rho}_s}{d\bar{t}}\right] + \frac{1}{2}\left(\bar{\rho}_b + \bar{\rho}_s - 2\right)\frac{d\bar{\delta}}{d\bar{t}} + \frac{3}{2}\left(\bar{\rho}_s - 1\right)\bar{\delta}\,\frac{d\bar{\delta}}{d\bar{t}} - 1$$

$$+ \left[\left(\bar{\rho}_b + \bar{\rho}_s\right)\bar{v}'_s - \frac{3}{2}\right]\bar{\delta} - \bar{\rho}_b\left(\bar{v}'_s - \bar{v}'_{b,S}\right)\frac{\bar{\delta}^2}{\bar{\delta}_S} = 0 \tag{A5}$$

This equation can be used to obtain an expression for the steady shock detachment ratio $\bar{\delta}_S$:

$$\bar{\delta}_S = \frac{1}{\bar{\rho}_{b,S}\bar{v}'_{b,S} + \rho_{s,S}\bar{v}'_s - \frac{3}{2}} \tag{A6}$$

The terms $d\bar{\rho}_b/d\bar{t}$ and $d\bar{\rho}_s/d\bar{t}$ in equation (A5) are neglected because there is little decompression in the stagnation region when $\gamma$ is near unity and $M_S$ is large. For example, the initial density ratio in the shock layer immediately after impingement is on the order of 11.00 when $\gamma = 1.1$ and $M_S = \infty$ ($M_\infty = 4.26$). The density ratios at the stagnation point and the shock are 10.49 and 10.00, respectively, for the steady case $\gamma = 1.1$ and $M_S = \infty$. The term which is proportional to $\bar{\delta}\,\frac{d\bar{\delta}}{d\bar{t}}$ is more than an order of

magnitude less than the term $\frac{1}{2}\left(\overline{\rho}_b + \overline{\rho}_s - 2\right)\frac{d\overline{\delta}}{d\overline{t}}$ when $\gamma$ is near unity and $M_S$ is large. Therefore, it is neglected.

The initial speed of the reflected shock is obtained by setting $\overline{\delta}$ equal to 0 in equation (A5):

$$\left(\frac{d\overline{\delta}}{d\overline{t}}\right)_{\overline{t}=0} = \left(\frac{2}{\overline{\rho}_b + \overline{\rho}_s - 2}\right)_{\overline{t}=0}$$

Since $\frac{2}{\overline{\rho}_b + \overline{\rho}_s - 2}$ changes very little throughout the period of unsteady flow, $\overline{c}$ is substituted for this quantity in equation (A5). The quantities $\left(\overline{\rho}_b + \overline{\rho}_s\right)\overline{v}'_s - \frac{3}{2}$ and $\overline{\rho}_b\left(\overline{v}'_s - \overline{v}'_{b,S}\right)\Big/\delta_S$ are assumed to be constant for the same reason.

When these approximations have been made, equation (A5) can be written in the form

$$\frac{d}{d\tau}\left(\frac{\delta}{\delta_S} - 1\right) + \alpha\left(\frac{\delta}{\delta_S} - 1\right) - (1 - \alpha)\left(\frac{\delta}{\delta_S} - 1\right)^2 = 0 \tag{A7}$$

where $\tau = \frac{ct}{\delta}$ and the quantity $\alpha$, which is constant, is given by

$$\alpha = \frac{2\overline{\rho}_{b,S}\overline{v}'_{b,S} - \left(\overline{\rho}_{b,S} - \overline{\rho}_{s,S}\right)\overline{v}'_s - \frac{3}{2}}{\overline{\rho}_{b,S}\overline{v}'_{b,S} + \overline{\rho}_{s,S}\overline{v}'_s - \frac{3}{2}} \tag{A8}$$

The solution to equation (A7) is

$$\frac{\delta}{\delta_S} = \frac{1 - e^{-\alpha\tau}}{1 - (1 - \alpha)e^{-\alpha\tau}} \tag{A9}$$

## REFERENCES


1. Cabannes, H.: Étude du départ d'un obstacle dans un fluide au repos (Écoulements plans – Écoulement de révolution). La Rech. Aeron., no. 36, Nov.-Dec. 1953, pp. 7-12.

2. Bausset, Max: Étude du départ d'un obstacle dans un fluide au repos. Compt. Rend., t. 261, no. 22, Nov. 29, 1965, pp. 4613-4616.

3. Miles, J. W.; Mirels, H.; and Wang, H. E.: Time Required for Establishing Detached Bow Shock. AIAA J. (Tech. Notes), vol. 4, no. 6, June 1966, pp. 1127-1128.

4. Davies, L.: Bow-Shock Establishment and Stagnation-Point Pressure Measurements for a Blunt-Nosed Body at Supersonic Speeds. NPL Aero Rept. 1098, Brit. A.R.C., Apr. 8, 1964.

5. Offenhartz, E.; and Weisblatt, H.: Determination of the Time History of the Flow Field About Blunt Bodies in a Shock Tube. Proceedings of Second Shock Tube Symposium, SWR-TM-58-3, U.S. Air Force, 1958, pp.119-130.

6. Bryson, A. E.; and Gross, R. W. F.: Diffraction of Strong Shocks by Cones, Cylinders, and Spheres. J. Fluid Mech., vol. 10, pt. 1, Feb. 1961, pp. 1-16.

7. Rutowski, R. W.; and Weimer, D.: Heat Transfer Measurements on a Hemisphere-Cylinder in the Lockheed Three-Inch Shock Tube. General Research in Flight Sciences. Volume I – Fluid Mechanics, LMSD-48381, Lockheed Missiles and Space Div., Jan. 1959, pp. 165-178.

8. Rabinowicz, Josef: Aerodynamic Studies in the Shock Tube. GALCIT Mem. No. 38 (Contract No. DA-04-495-Ord-19), June 10, 1957.

9. Butler, Thomas Daniel: Numerical Calculations of the Transient Loading of Blunt Obstacles by Shocks in Air. AIAA J., vol. 4, no. 3, Mar. 1966, pp. 460-467.

10. Lax, Peter D.: Weak Solutions of Nonlinear Hyperbolic Equations and Their Numerical Computation. Commun. Pure Appl. Math., vol. VII, no. 1, Feb. 1954, pp. 159-193.

11. Bohachevsky, Ihor O.; and Rubin, Ephraim L.: A Direct Method for Computation of Nonequilibrium Flows With Detached Shock Waves. AIAA J., vol. 4, no. 4, Apr. 1966, pp. 600-607.

12. Bohachevsky, Ihor O.; and Mates, Robert E.: A Direct Method for Calculation of the Flow About an Axisymmetric Blunt Body at Angle of Attack. AIAA J., vol. 4, no. 5, May 1966, pp. 776-782.

13. Roberts, Leonard: On the Numerical Solution of the Equations for Spherical Waves of Finite Amplitude, II. J. Math. Phys., vol. XXXVI, no. 4, Jan. 1958, pp. 329-337.

14. DeJarnette, Fred R.: Application of Lax's Finite-Difference Method to Nonequilibrium Hypersonic Flow Problems. NASA TR R-234, 1966.

15. Courant, R.; Friedrichs, K.; and Lewy, H.: Über die partiellen Differenzengleichungen der mathematischen Physik. Math. Ann., vol. 100, 1928, pp. 32-74.

16. Lighthill, M. J.: The Diffraction of Blast. II. Proc. Roy. Soc. (London), ser. A, vol. 200, no. 1063, Feb. 22, 1950, pp. 554-565.

17. Courant, R.; and Friedrichs, K. O.: Supersonic Flow and Shock Waves. Interscience Publ., Inc. (New York), 1948, p. 341.

18. Ladenburg, R.; Winckler, J.; and Van Voorhis, C. C.: Interferometric Studies of Faster Than Sound Phenomena. Part I. The Gas Flow Around Various Objects in a Free, Homogeneous, Supersonic Air Stream. Phys. Rev., vol. 73, no. 11, June 1, 1948, pp. 1359-1377.

19. Kendall, James M., Jr.: Experiments on Supersonic Blunt-Body Flows. Progr. Rept. No. 20-372 (Contract No. DA-04-495-Ord 18), Jet Propulsion Lab., California Inst. Technol., Feb. 27, 1959.

20. Van Dyke, Milton D.; and Gordon, Helen D.: Supersonic Flow Past a Family of Blunt Axisymmetric Bodies. NASA TR R-1, 1959.

21. Lomax, Harvard; and Inouye, Mamoru: Numerical Analysis of Flow Properties About Blunt Bodies Moving at Supersonic Speeds in an Equilibrium Gas. NASA TR R-204, 1964.

22. Belotserkovskii, O. M.: Flow With a Detached Shock Wave About a Symmetrical Profile. J. Appl. Math. Mech., vol. 22, no. 2, 1958, pp. 279-296.

*"The aeronautical and space activities of the United States shall be conducted so as to contribute . . . to the expansion of human knowledge of phenomena in the atmosphere and space. The Administration shall provide for the widest practicable and appropriate dissemination of information concerning its activities and the results thereof."*

—NATIONAL AERONAUTICS AND SPACE ACT OF 1958

# NASA SCIENTIFIC AND TECHNICAL PUBLICATIONS

TECHNICAL REPORTS: Scientific and technical information considered important, complete, and a lasting contribution to existing knowledge.

TECHNICAL NOTES: Information less broad in scope but nevertheless of importance as a contribution to existing knowledge.

TECHNICAL MEMORANDUMS: Information receiving limited distribution because of preliminary data, security classification, or other reasons.

CONTRACTOR REPORTS: Scientific and technical information generated under a NASA contract or grant and considered an important contribution to existing knowledge.

TECHNICAL TRANSLATIONS: Information published in a foreign language considered to merit NASA distribution in English.

SPECIAL PUBLICATIONS: Information derived from or of value to NASA activities. Publications include conference proceedings, monographs, data compilations, handbooks, sourcebooks, and special bibliographies.

TECHNOLOGY UTILIZATION PUBLICATIONS: Information on technology used by NASA that may be of particular interest in commercial and other non-aerospace applications. Publications include Tech Briefs, Technology Utilization Reports and Notes, and Technology Surveys.

***Details on the availability of these publications may be obtained from:***

SCIENTIFIC AND TECHNICAL INFORMATION DIVISION

NATIONAL AERONAUTICS AND SPACE ADMINISTRATION

**Washington, D.C. 20546**